Published in final edited form as:
J Comp Neurol. 2013 August 1; 521(11): 2538–2550. doi:10.1002/cne.23297.

Differential Connectivity of Short- Vs. Long-Range Extrinsic and Intrinsic Cortical Inputs to Perirhinal Neurons

Gunes Unal[1], **Jean-Francois Pare**[2], **Yoland Smith**[2], and **Denis Pare**[1,*]

[1]Center for Molecular and Behavioral Neuroscience, Rutgers University, Newark, New Jersey 07102

[2]Yerkes National Primate Research Center and Department of Neurology, Emory University, Atlanta, Georgia 30329

Abstract

The perirhinal cortex plays a critical role in recognition and associative memory. However, the network properties that support perirhinal contributions to memory are unclear. To shed light on this question, we compared the synaptic articulation of short- and long-range inputs from the perirhinal cortex or temporal neocortex with perirhinal neurons in rats. Iontophoretic injections of the anterograde tracer *Phaseolus vulgaris*-leucoagglutinin (PHAL) were performed at different rostrocaudal levels of the ventral temporal neocortex or perirhinal cortex, and electron microscopic observations of anterogradely labeled ($PHAL^+$) axon terminals found at perirhinal sites adjacent to or rostrocaudally distant from the injection sites were performed. After neocortical injections, the density of $PHAL^+$ axons in the perirhinal cortex decreased steeply with rostrocaudal distance from the injection sites, much more so than following perirhinal injections. Otherwise, similar results were obtained with neocortical and perirhinal injections. In both cases, most (76–86%) $PHAL^+$ axon terminals formed asymmetric synapses, typically with spines (type A, 83–89%) and less frequently with dendritic profiles (type B, 11–17%). The remaining terminals formed symmetric synapses with dendritic profiles (type C, 14– 23%). Type B and C synapses were 2.4–2.6 times more frequent in short- than long-range connections. The postsynaptic elements in type A–C synapses were identified with immunocytochemistry for CAMKIIa, a marker of glutamatergic cortical neurons. Type A and C terminals contacted CAMKII α- positive principal cells, whereas type B synapses contacted presumed inhibitory neurons. Overall, these results suggest that principal perirhinal neurons are subjected to significantly more inhibition from short- than from long-range cortical inputs, an organization that likely impacts perirhinal contributions to memory.

Indexing Terms

perirhinal; GABA; interneuron; electron microscopy; tract-tracing

*Correspondence TO: Denis Pare, Center for Molecular and Behavioral Neuroscience, Rutgers State University, 197 University Ave., Newark, NJ 07102. pare@andromeda.rutgers.edu.

Conflict Of Interest Statement: The authors have no conflict of interest, financial or otherwise.

Role Of Authors: All authors had full access to all the data in the study and take responsibility for the integrity of the data and the accuracy of the data analysis. Study concept and design: DP, YS, GU. Acquisition of data: GU, JFP. Analysis and interpretation of data: DP, YS, GU, JFP. Drafting of the manuscript: DP. Critical revision of the manuscript for important intellectual content: YS, GU. Statistical analysis: GU, DP. Obtained funding: DP, YS. Administrative, technical, and material support: JFP. Study supervision: DP, YS.

The perirhinal cortex (PRC) plays a critical role in recognition and associative memory (for review see Suzuki, 1996). Accordingly, it receives inputs from high-order associative cortical areas (Deacon et al., 1983; Room and Groenewegen, 1986; Suzuki and Amaral, 1994; Burwell and Amaral, 1998a), most of which originate from a strip of cortex, hereafter termed the *ventral temporal association cortex* (VTAC), that borders the PRC laterally. These inputs are organized topographically, with anterior VTAC mainly targeting rostral perirhinal levels and caudal VTAC focusing on posterior perirhinal sectors. Superimposed on these transversely organized VTAC inputs is a prominent system of longitudinal connections (Witter et al., 1986; Burwell and Amaral, 1989b; Lavenex et al., 2004) that supports the rostrocaudal propagation of neocortical influences in the perirhinal cortex (Biella et al., 2001, 2010; Martina et al., 2001). Most of these originate in perirhinal neurons themselves, but some neocortical cells contribute as well (Deacon et al., 1983; Room and Groenewegen, 1986).

Electrophysiological studies suggest that short- and long-range cortical inputs to perirhinal neurons form contrasting connections with local-circuit and principal perirhinal cells. Indeed, VTAC stimuli applied in rostrocaudal register with the recorded perirhinal cells evoke large inhibitory postsynaptic potentials (IPSPs) that curtail the initial excitatory postsynaptic potentials (EPSPs). In contrast, VTAC stimuli delivered at rostrocaudally distant sites evoke apparently pure excitatory responses (Biella et al., 2001; Martina et al., 2001). These findings were interpreted as evidence that short-range inputs recruit local-circuit cells more strongly than long-range connections.

The significance of this interpretation comes from earlier studies on the neuronal correlates of recognition and associative memory formation. Recognition memory depends on a *reduction* in the responsiveness of perirhinal neurons to familiar stimuli (Brown et al., 1987; Fahy et al., 1993; Li et al., 1993; Miller et al., 1993; Sobotka and Ringo, 1993). In contrast, associative memory formation is linked to *increasing* responses of perirhinal neurons to paired stimuli (Messinger et al., 2001; Naya et al., 2003a). However, it is currently unclear why repeated presentations of one vs. two stimuli lead to opposite changes in the responsiveness of perirhinal neurons.

Based on the differential connectivity of short- vs. long-range pathways and the finding that VTAC inputs can be depressed or potentiated depending on the membrane potential of target cells (Cho et al., 2001), it was proposed that the fate of VTAC inputs (depression vs. potentiation) depends on whether perirhinal cells receiving short-range VTAC inputs also receive convergent inputs from long-range pathways (Unal et al., 2012). Consistent with this, it was reported that repeated activation of one set of VTAC inputs causes a depression of evoked responses, whereas activation of distributed VTAC inputs elicits a potentiation of the responses evoked by the paired stimuli (Unal et al., 2012).

However, these views are entirely based on the interpretation of physiological findings. There is no anatomical evidence that the perirhinal circuit is, indeed, organized in this manner. Thus, the present study was undertaken to directly test whether short- and long-range cortical inputs to the PRC are connected differentially with local-circuit cells. This issue was addressed in rats using anterograde tracing of short- and long-range connections from the VTAC or PRC coupled to CAMKIIa immunocytochemistry at the light and electron microscopic (EM) level.

Materials and Methods

Tract tracing

The surgical procedures used in this study were in accordance with the NIH *Guide for the care and use of laboratory animals* and were approved by the institutional animal care and use committee at Rutgers and Emory Universities. In total, 36 adult male Sprague-Dawley rats weighing 220-320 g were used in this study. The animals were kept on a 12-hour light/dark cycle and had free access to food and water. They were anesthetized with isoflurane and administered atropine (0.05 mg/kg, i.m.) to reduce salivation. After placing the rats in a stereotaxic apparatus and shaving their scalp, we made numerous, evenly spaced, small injections of the analgesic bupivacaine (0.125% solution, s.c.) around the sites to be incised. Ten minutes later, under sterile conditions, the scalp was incised above the cortical regions of interest, small openings were drilled into the skull, and the dura mater was opened.

The rats then received unilateral injections of the anterograde tracer *Phaseolus vulgaris*-leucoagglutinin (PHAL; Vector, Burlingame, CA) aimed at different rostrocaudal levels of the VTAC or PRC. PHAL was dissolved as a 2.5% solution in 0.01 M phosphate buffer, pH 8.0, and injected iontophoretically through a glass pipette (tip diameter 25–30 lm) using positive 7-μA current pulses, on and off every 7 sec for 15 min. The injections were aimed at four sites (coordinates in millimeters relative to bregma): a rostral PRC level (AP, −3.3; ML, 6.3; DV, −4.6), a caudal PRC level (AP, −5.2; ML, 7.1; DV, −4.1), a rostral VTAC level (AP, −3.3; ML, 6.3; DV, −3.2), and finally a caudal VTAC (AP, −5.2; ML, 7.1; DV, −3.1). These coordinates were determined by using a stereotaxic atlas of the rat brain (Paxinos and Watson, 2007). Rostral and caudal VTAC regions correspond to the ventral portion of the secondary auditory cortex and temporal association cortex, respectively (Paxinos and Watson, 2007). To provide a sufficient amount of labeled terminals to be examined in the electron microscope, we performed relatively large PHAL injections, which involved both superficial and deep cortical layers of PRC (areas 36 and 35) and VTAC.

After a survival period of 10–12 days, the animals were deeply anesthetized with sodium pentobarbital (50 mg/kg, i.p.) and perfused through the heart with 50–100 ml of 0.9% saline, followed by 500 ml of a fixative containing 0.1%glutaraldehyde and 4% depolymerized paraformaldehyde in 0.1 M phosphate buffer, pH 7.4 (PB). The brains were removed, cut into blocks containing the perirhinal cortex, and postfixed in the same fixative overnight. The tissue blocks were then sectioned at 60 μm using a vibrating microtome and collected in PBS.

Immunocytochemical procedures

In all cases, PHAL was detected with the immunoperoxidase method, whereas CAMKIIα immunoreactivity was detected using the pre-embedding immunogold-silver intensification procedure. It should be noted that no differentiated labeling was seen when the PHAL antibody was used on brain sections obtained from animals that did not receive PHAL injections. We used a mouse monoclonal (6G9) anti-CaMKIIa antibody (Abcam, Cambridge, MA; catalog AB22609, lot GR30131-1). This antibody was prepared against purified CaMKIIa. It was evaluated by Abcam for activity and specificity. Western blot analysis gave positive signals in human, rat, and mouse whole-brain tissue lysates, detected as a band with a molecular weight of 50 kDa. This antibody detects CaMKIIa in its phosphorylated and nonphosphorylated forms (Erondu and Kennedy, 1985; Jung et al., 2008).

To reveal PHAL, sections were incubated in sodium borohydride (1% in PBS) for 20 min at room temperature, rinsed repeatedly in PBS (0.01 M, pH 7.4), and incubated for 60 min in a

blocking solution. The blocking solution contained 1% BSA, 1% normal goat serum (NGS), and 0.03% Triton X-100 in PBS. The sections were then incubated overnight in rabbit anti-PHAL (1:1,000; Vector). On the next day, the sections were rinsed in PBS (3 × 10 min), then incubated for 90 min in biotinylated goat anti-rabbit IgG (1:200; Vector) and rinsed in PBS (3 × 10 min). Finally, the sections were incubated for 90 min in the avidin-biotin peroxidase complex (ABC; Vector). The peroxidase was revealed using a solution of 0.025% diaminobenzidine (DAB) and 0.006% hydrogen peroxide in TBS. The sections were then rinsed in 0.01 M PBS (pH 7.4). At the end of the incubations, the sections were mounted onto glass slides, air dried, and dehydrated in a graded series of alcohol. Finally, the glass slides were coverslipped in Permount mounting medium (Fisher Scientific, Pittsburgh, PA) for light microscopic observations.

For electron microscopy, the sections were placed in a cryoprotectant solution (25% sucrose and 10% glycerol in PB, 0.05 M, pH 7.4) for 20 min. To facilitate antibody penetration, they were then placed in a −80°C freezer for an additional 20 min to permeabilize cell membranes, thawed, and washed in PBS before being processed for immunocytochemistry. The sections were then processed as described above with the exception that Triton X-100 was not used and that the incubation with the primary antibody lasted for 48 hours at 4°C. Next, they were rinsed in PB, postfixed in osmium tetroxide (1% in PB) for 20 min, and rinsed several times in PB. Then, the sections were dehydrated in graded series of alcohol and propylene oxide. Uranyl acetate (1%) was added to the 70% alcohol for 35 minutes to improve contrast in the electron microscope. Finally, they were embedded in Durcupan resin (Fluka, Gymea, Australia), transferred to glass slides, coverslipped, and left in the oven at 60°C for 48 hours. After resin polymerization, the regions of interest were cut and removed from the glass, stuck on resin blocks, and trimmed in a trapezoidal shape before being cut with an ultramicrotome (Ultracut-T; Leica Microsystems, Wetzlar, Germany). These blocks were sectioned at 60–70 nm with a 45°-diamond knife. Ultrathin sections were then collected onto copper single-slot grids. Finally, sections were counterstained with Reynold's lead citrate, air dried, and stored in grid boxes for electron microscopic analysis.

The following procedure was used to localize both PHAL and CaMKIIα immunoreactivity in the same sections. First, the sections were incubated in sodium borohydride (1% in PBS) for 20 min at room temperature and rinsed repeatedly with PBS. Then, they were placed in a cryoprotectant solution as described above. Once the sections were brought back to room temperature, they were preincubated in a PBS solution containing 5% milk for 30 min, rinsed in TBS-gelatin (pH 7.6, 3 × 5 min), and incubated overnight in a TBS-gelatin solution containing 1% milk, and a cocktail of mouse anti-CaMKII (1:4,000; Abcam, Cambridge, MA) and rabbit anti-PHAL antibodies (1:1,000; Vector). The sections were then rinsed in TBS-gelatin (3 × 10 min) and incubated for 2 hours in gold-conjugated goat anti-mouse IgGs (1:100; Nanogold; Nanoprobes, Stonybrook, NY) and in biotinylated goat anti-rabbit IgGs (1:200; Vector) in a TBS-gelatin solution containing 1% milk. After the incubation, the sections were rinsed with TBS-gelatin (2 × 10 min) and a 2% aqueous acetate buffer solution (pH 7.0) for 10 min. Then, they were transferred to a darkroom for silver intensification of gold particles for 8–10 min with the HQ silver kit (Nanoprobes). After intensification, the sections were rinsed repeatedly in acetate buffer and in TBS-gelatin for 10 min. Then, they were incubated with the ABC solution in TBS-gelatin with 1% milk for 90 min and rinsed in TBS-gelatin (2 × 10 min) and in Tris buffer for 10 min. The sections were then incubated in DAB (0.025%) for 10 min at room temperature, rinsed thoroughly in PBS, and transferred in 0.1M PB (pH 7.4) for 5 min. The remaining steps were as described above with the exception that we used 0.5% osmium tetroxide for 10 min and uranyl acetate for 10 min.

First, slides prepared for light microscopy were examined to determine the location of the PHAL injections in each animal. Only tissue from animals with injection sites restricted to the targeted locations (i.e., PRC or VTAC), with no diffusion to nearby regions, were included in the data analysis. For each successful PHAL injection site, and in each region of interest, two to four blocks of tissue were examined, depending on the density of labeled terminals that could be analyzed per block. Selected sections were photographed, and the area of interest was drawn on the photographs. The tissue blocks were then cut into 70-nm-thick sections that were collected onto copper single-slot grids. Only the most superficial ultrathin sections of the blocks were considered to ensure optimal penetration of the antibodies. Grids were examined in a transmission electron microscope (100 kV; × 10,000-60,000; JEM-1011; JEOL, Peabody, MA), and micrographs were digitally imaged by an 11-megapixel lens-coupled CCD camera (ES1000W; Gatan, Warrendale, PA). The observer was blind to the location of the PHAL injection sites and the source of the tissue blocks used for electron microscopic observations.

Data analysis

Each section was scanned for PHAL-labeled terminals forming clear synaptic contacts with well-defined postsynaptic elements. Labeled terminals were recognized by the presence of the amorphous electron-dense peroxidase reaction product. We used the ultrastructural criteria defined by Peters et al. (1991) to categorize postsynaptic elements. Spines could be readily identified as such when they were seen to emerge from the parent dendrite. When the spine and parent dendrite were not located in the same plane, spines were identified by the presence of a spine apparatus, as well as the lack of microtubules and mitochondria, whereas dendritic shafts were generally larger and included microtubules, mitochondria, endoplasmic reticulum, or a combination of these structures.

For each animal, 100 labeled terminals were identified and digitally captured from two locations in the PRC: half of the micrographs were taken close to the injection site (≤1 mm), and the other half were taken from distant sites (>1 mm). In the cases of PRC injections, a section was considered to be a “close site” if PHAL-labeled somata could be detected within 1 mm in the AP axis. In these areas, sections were taken ≥200 μm away from labeled somata, to ensure that observations targeted regions well outside the injection site. In the cases of VTAC injections, micrographs taken from PRC levels in transverse register with the injection site were considered to be a close site. To be considered a “distant site,” the observed region had to be at least 1 mm away from the perirhinal region in transverse register with the neocortical injection site, sometimes as far as 2.5 mm. For cases with rostral injection sites (AP, −3.3), the distant sites were taken from more caudal PRC levels. For cases with caudal injection sites (AP, −5.2), the distant sites were taken from more rostral PRC levels.

Photomicrographs of labeled terminals were cropped into Adobe Photoshop CS5 (Adobe Systems, San Jose, CA). Brightness and contrast adjustments were performed with the same software to ensure uniformity in multipanel figures. However, such adjustments were applied to the entire image. The photographs were then imported in Adobe Illustrator CS5 to add labels and scale bars.

Results

Location of injection sites and light microscopic observations

Among the 36 animals, eight received PHAL injections confined to regions of interest: two in rostral PRC, two in caudal PRC, two in rostral VTAC, and two in caudal VTAC. The following results are based on the analysis of labeling in these eight cases. Figure 1 shows

darkfield photomicrographs of representative perirhinal (Fig. 1A) and VTAC (Fig. 1D) injection sites and of the resulting anterograde labeling in area 35 of the PRC (Fig. 1B,E). Note that, with both types of injections, PHAL-labeled axons contributed numerous en passant and terminal varicosities in all target regions examined (Fig. 1C,F).

Figure 2 compares the pattern of anterograde labeling seen in the PRC after the perirhinal (Fig. 2A,B) and VTAC (Fig. 2C,D) injections shown in Figure 1A and D, respectively. In both cases, the left section (Fig. 2A,C) is adjacent, but slightly rostral, to the PHAL injection site, whereas the right section (Fig. 2B,D) shows labeling at a level of the PRC that is rostrocaudally distant from the injection site. Consistent with earlier descriptions (Deacon et al., 1983; Room and Groenewegen, 1986; Witter et al., 1986; Lavenex et al., 2004; Pinto et al., 2006), the PRC injection (Fig. 1A) produced pronounced labeling of intrinsic longitudinal perirhinal axons (Fig. 2B). Notably, whether the PHAL injections targeted rostral or caudal levels of the PRC, we observed little attenuation in the density of PHAL-labeled perirhinal axons with rostrocaudal distance from the injection site (compare Fig. 2A,B). In contrast, after PHAL injections in the VTAC (Fig. 1D), a marked attenuation in labeling intensity was seen with distance. Indeed, at levels adjacent to the injection site (Fig. 2C), dense labeling was seen in area 36 and moderate labeling in area 35. In contrast, at rostrocaudally distant sites (Fig. 2D), markedly fewer PHAL-immunoreactive axons were present in perirhinal areas 36 and 35.

Electron microscopic observations

The sections prepared for electron microscopic observations were first examined in the light microscope to identify areas containing dense anterograde labeling. In the electron microscope, the sections were scanned for the presence of PHAL-immunoreactive axon terminals. PHAL-labeled structures were easy to differentiate from unlabeled elements because of the electron-dense, amorphous DAB reaction product associated with them. In the PRC, the DAB reaction product occurred in nonmyelinated axons and presynaptic boutons, where it was associated with the external surface of microtubules, electron-lucent vesicles, and mitochondria as well as with the internal surface of the plasmalemma.

For each of the eight PHAL injections confined to the PRC or VTAC, we analyzed the synaptic connections of 50 terminals in perirhinal sectors either adjacent to or rostrocaudally distant from the injection sites. Whenever possible, all 50 terminals were analyzed from the same grid. However, in some cases, especially at perirhinal sites distant from the VTAC injections, several grids were required to collect 50 terminals because of the lower density of labeled boutons. Overall, we analyzed the pattern of synaptic connections formed by a total of 800 PHAL-labeled terminals distributed equally across the eight animals used in this study. Figure 3 summarizes the distribution of postsynaptic elements to these terminals following PRC or VTAC injections. Figure 4 shows representative examples of these terminals.

Synaptic connections of short- and long-range intrinsic perirhinal axons

Our electron microscopic observations revealed similarities as well as interesting differences in the synaptic connections of short- and long-range perirhinal axons (Fig. 3). In both cases, a majority of PHAL-positive terminals formed asymmetric synapses (66.5% and 86% for short- and long-range projections, respectively), typically with dendritic spines (82% and 94.2% for short- and long-range projections, respectively). An example of such axospinous synapses is illustrated in Figure 4A. In light of previous work on the general ultrastructure of the cerebral cortex in general (Colonnier, 1981; Peters et al., 1991; DeFelipe and Fariñas, 1992) and of the rhinal cortices in particular (here defined as peri-, post-, and entorhinal cortices; Smith and Pare, 1994; Wouterlood et al., 2000, 2004; van Haeften et al., 2003;

Pinto et al., 2006), such asymmetric axospinous synapses likely represent excitatory (glutamatergic) inputs to principal perirhinal neurons.

Although spines constituted the main targets of short-and long-range perirhinal connections, the proportion of asymmetric synapses targeting spines vs. dendritic shafts differed significantly in the two pathways. Indeed, short-range projections formed a significantly higher proportion of asymmetric synapses with dendritic profiles (18.1%) compared with long-range projections (5.8%; χ^2-test, $P = 0.0008$). Moreover, whereas symmetric synapses constituted a substantial proportion of synapses in both short-and long-range connections, the proportion of symmetric synapses found in short-range projections was more than twice that seen in the long-range projections (33.5% and 14% for short- and long-range projections, respectively; χ^2-test, $P < 0.0001$). However, in both cases, the postsynaptic elements in these symmetric synapses were almost exclusively dendritic shafts (Fig. 3). An example of such a symmetric synapse is shown in Figure 4B.

Synaptic connections of short- and long-range VTAC projections to the perirhinal cortex

The pattern of results obtained in VTAC projections closely paralleled that described above for intrinsic perirhinal connections. The majority of short- and long-range PHAL-positive neocortical axons formed asymmetric synapses (76% and 96%, respectively), predominantly with dendritic spines (77.6% and 87.5% for short- and long-range projections, respectively), as described for intrinsic perirhinal axons. An example of an axospinous synapse formed by temporal neocortical projections to the PRC is illustrated in Figure 4C. Also reminiscent of the results obtained with intrinsic perirhinal projections, VTAC axons projecting to nearby perirhinal sites formed a significantly higher proportion of asymmetric synapses with dendritic profiles (22.4%) than those projecting to distant sites (12.5%; χ^2-test, $P = 0.016$; Fig. 3).

The difference in the incidence of symmetric synapses identified in short- vs. long-range perirhinal connections was also apparent in VTAC projections to nearby vs. longitudinally distant perirhinal sites. Indeed, at perirhinal levels adjacent to the VTAC injection site, for instance, as many as 24% of PHAL-positive axon terminals formed symmetric synapses, compared with only 4% in long-range connections (χ^2-test, $P < 0.0001$; Fig. 3). However, in both cases, the postsynaptic elements in these symmetric synapses were almost exclusively dendritic shafts (Fig. 3). An example of a symmetric synapse formed by a PHAL-labeled VTAC axon terminal is displayed in Figure 4D.

In closing this section, it is important to emphasize that the pattern of results described above for VTAC and perirhinal projections did not depend on whether the PHAL injections were performed at rostral or caudal levels. For instance, no significant differences were found between the proportions of symmetric synapses formed at close vs. distant sites following PHAL injections in rostral vs. caudal levels of the VTAC (χ^2-test, $P = 0.21$) or PRC (χ^2-test, $P = 0.27$).

Relationships between PHAL-labeled terminals and CaMKIIα-immunoreactive perirhinal neurons

The significance of the differences between the connections formed by short- and long-range PRC and VTAC axons depends on the identity of their targets. Fortunately, a large body of ultrastructural data is available to guide our interpretations (for reviews see Colonnier, 1981; Peters et al., 1991; DeFelipe and Fariñas, 1992; for papers on the ultrastructure of the rhinal cortices see Smith and Pare, 1994; Wouterlood et al., 2000, 2004; van Haeften et al., 2003; Pinto et al., 2006). A first critical clue resides in the fact that inhibitory interneurons are aspiny or sparsely spiny, whereas principal cells are densely

covered with spines. Second, it is well established that almost all asymmetric synapses to principal cells end on dendritic spines. As a result, it is customary in the cortical literature to interpret asymmetric axospinous and axodendritic synapses as representing excitatory inputs to principal cells vs. local-circuit neurons, respectively. On the other hand, the identity of the post-synaptic elements in symmetric synapses is not as clear, because such synapses end on the dendritic shafts of both principal cells and local-circuit neurons.

To shed light on this question, we took advantage of the fact that, in the cerebral cortex, the type II alpha subunit of calcium/calmodulin-dependent protein kinase (CaMKIIα) is strongly expressed in principal cells but is absent from GABAergic interneurons (Benson et al., 1992; Tighilet et al., 1998). Thus, by using pre-embedding immunocytochemistry to detect neuronal elements expressing CaMKIIα, we first looked for spiny dendritic shafts that were parallel to the plane of the ultrathin sections and assessed whether CaMKIIα was expressed in these dendrites. Consistent with previous observations (Benson et al., 1992; Tighilet et al., 1998), 100% of the 30 spiny dendrites that we observed were strongly immunoreactive for CaMKIIα (Fig. 5A–C), while aspiny dendritic profiles devoid of CaMKIIα immunoreactivity were frequently observed in the same material (Fig. 5C, u-d).

Having established that CaMKIIα immunoreactivity constitutes a reliable approach to identify positively dendritic profiles belonging to principal neurons, we next examined the synaptic relationships between PHAL-labeled terminals and CaMKIIα-immunoreactive dendrites. To do so, superficial ultrathin sections from four different animals with PHAL injections in the VTAC or PRC were obtained from perirhinal areas adjacent to the injection sites. As described above, these areas exhibit the highest prevalence of PHAL-labeled terminals in contact with dendritic shafts (Fig. 3). As shown in Figure 6A,B, this analysis revealed that the symmetric axodendritic synapses formed by PHAL-positive axon terminals involved CaMKIIα-positive dendritic shafts (n = 16). By contrast, in every case in which a PHAL-positive axon terminal was seen to form an asymmetric synapse onto a dendritic shaft (n = 27), the postsynaptic element was immunonegative for CaMKIIα (Fig. 6C). Thus, these results suggest that, in short-range VTAC and PRC projections, asymmetric synapses onto dendritic shafts represent excitatory synapses onto putative local-circuit cells, whereas symmetric synapses onto dendritic shafts are inhibitory synapses onto principal cells.

Discussion

The present study was undertaken to shed light on the distinguishing network properties that support perirhinal contributions to memory. To this end, we used anterograde tracing with PHAL coupled with immunocytochemistry for CaMKIIα, a protein kinase that is expressed by principal, but not local-circuit, cortical neurons (Benson et al., 1992; Tighilet et al., 1998). With the electron microscope, we compared the type of synapses formed by VTAC and PRC axons with perirhinal cells located at sites adjacent to (short-range pathways) vs. rostrocaudally distant from (long-range pathways) the PHAL injections. Overall, the results obtained with PHAL deposits in the VTAC or PRC support the same conclusion: short-range pathways give rise to a larger contingent of inhibitory connections to PRC than long-range pathways (Fig. 7A). In both cases, this inhibition takes two forms: 1) principal VTAC or perirhinal cells forming excitatory synapses with local-circuit inhibitory neurons of the PRC (Fig. 7A1) and 2) inhibitory neurons of the VTAC or PRC contacting principal perirhinal cells (Fig. 7A2). The significance of these findings for perirhinal contributions to memory is discussed below.

Recruitment of inhibition by cortical inputs to the perirhinal cortex

Previous tracing studies have shown that a proportion of VTAC and PRC neurons contributes longitudinal axons in the PRC (Deacon et al., 1983; Room and Groenewegen,

1986; Witter et al., 1986; Burwell and Amaral, 1998b; Lavenex et al., 2004). However, as revealed in the present study, VTAC contributions to these longitudinal pathways are less prominent than those of perirhinal cells. This statement is based on the observation that the density of anterograde labeling in the PRC decreased more steeply with rostrocaudal distance from the injection site following PHAL injections in the VTAC than in the PRC.

Nevertheless, electrophysiological studies have reported that localized VTAC stimuli elicit neuronal responses that propagate throughout the rostrocaudal extent of the PRC, albeit with some attenuation (Biella et al., 2001, 2010; Martina et al., 2001; Unal et al., 2012). This propagation was found to depend on longitudinal axonal pathways coursing in the perirhinal cortex itself and/or the external capsule, not in the VTAC. Indeed, interruption of intrinsic perirhinal pathways with restricted knife cuts (Martina et al., 2001) or their inactivation with local injections of lidocaine (Unal et al., 2012) prevented the propagation, whereas these interventions in the VTAC had no effect.

In the same studies, it was noted that the impact of VTAC stimuli on perirhinal cells varies with longitudinal distance between the stimulation and recording sites (Biella et al., 2001; Martina et al., 2001). VTAC stimuli applied at the same rostrocaudal level as the recorded cells evoke large IPSPs that counter the initial EPSP. By contrast, stimulation of rostrocaudally distant sites apparently triggers pure excitatory responses. This led to the suggestion that short-range pathways strongly recruit local-circuit cells of the PRC, much more so than long-range pathways, leading to a powerful feed-forward inhibition of principal cells.

The present study provides support for this interpretation by showing that inhibition is a much more important component of the short- than of the long-range pathways contributed by VTAC and perirhinal neurons (Fig. 7A). Indeed, asymmetric synapses onto dendritic spines, which presumably represent glutamatergic inputs to principal perirhinal cells, accounted for the vast majority (>80%) of the synapses seen in long-range pathways compared with ∼55% for short-range pathways. The lower proportion of excitatory inputs to principal cells in short-range pathways is due to two factors. First, asymmetric synapses onto CaMKIIα-negative dendritic shafts, which represent mainly glutamatergic inputs to local-circuits cells, were nearly twice as frequent in short- as in long-range pathways. Second, the proportion of symmetric synapses formed with dendritic shafts, most of which were CaMKIIα-positive and probably represent inhibitory inputs onto principal cells, were seen approximately three times more frequently in short- than in long-range pathways.

Although it is not surprising that the axons of local-circuit perirhinal neurons show limited anteroposterior divergence, the fact that GABAergic cells of the VTAC also contribute axon terminals in the PRC is inconsistent with the classical model of cortical physiology. According to this model, communication between cortical areas depends on glutamatergic neurons, with inhibitory cells acting locally, within the area where their somata are located. Consequently, according to this view, IPSPs generated in the course of interareal cortical interactions are thought to arise disynaptically, after the glutamatergic activation of local-circuit GABAergic neurons.

Although the finding that the VTAC contains long-range GABAergic neurons runs counter to the classical model of cortical inhibition, there are many precedents for this observation in the literature. For instance, some GABAergic neurons of the visual cortex project to the contralateral visual cortex (Hughes and Peters, 1992). Some hippocampal interneurons in field CA1 contribute long-range projections to field CA3 (Sik et al., 1994), and some dentate GABAergic neuron project to the subiculum (Ceranik et al., 1997). Similarly, some entorhinal neurons projecting to the dentate gyrus are GABAergic (Germroth et al., 1989),

and there are GABAergic projections from the presubiculum to the entorhinal cortex (Van Haeften et al., 1997). Finally, it has been reported that the PRC contains a population of long-range GABAergic cells that projects to the entorhinal cortex (Pinto et al., 2006; Apergis-Schoute et al., 2007).

Significance for perirhinal contribution to memory

Previously, an interesting parallel was noted between the cellular correlates of memory formation in the PRC and in vitro studies of PRC plasticity (Unal et al., 2012). In vivo, it was observed that repeated presentations of the same or two different stimuli have opposite effects on perirhinal responses to the repeatedly presented stimuli. Repeated presentations of one stimulus cause a long-term reduction of perirhinal responses evoked by that stimulus (Brown et al., 1987; Fahy et al., 1993; Li et al., 1993; Miller et al., 1993; Sobotka and Ringo, 1993; Messinger et al., 2001; Naya et al., 2003). This phenomenon, known as *familiarity-induced response depression*, was also seen in human functional imaging studies (Litman et al., 2009). In contrast, an opposite behavior is observed when monkeys are trained to form associations between two arbitrary visual stimuli (Messinger et al., 2001; Naya et al., 2003). Initially, many perirhinal neurons responded selectively to some of the stimuli. How- ever, as a result of training, many of the same neurons also became preferentially activated by the paired associate stimulus. Thus, in this case, with repeated presentations of two stimuli, perirhinal responses increased.

In vitro studies of activity-dependent perirhinal plasticity parallel these in vivo findings. Indeed, repeated activation of a spatially restricted set of VTAC inputs in vitro induces long-term depression (LTD) of PRC responses (Fig. 7B), whereas repeated pairings of spatially distributed VTAC inputs have the opposite effect (Fig. 7C; long-term potentiation, LTP; Unal et al., 2012). These two forms of plasticity depend on the competing influence of group I metabotropic glutamate and N-methyl-D-aspartate (NMDA) receptors, respectively.

Based on the differential recruitment of inhibition by short- vs. long-range pathways, it was proposed that the fate of VTAC inputs (LTD or LTP) depends on whether principal perirhinal cells receiving short-range VTAC inputs also receive convergent inputs from long-range perirhinal pathways (Fig. 7B,C; Unal et al., 2012). By shifting the excitatory–inhibitory balance toward excitation, the convergence of short- and long-range inputs would remove the Mg^{2+} block of NMDA receptors, leading to the induction of NMDAR-dependent LTP. In contrast, when short-range pathways are repeatedly activated in isolation, this would lead to LTD.

However, these views were based entirely on the interpretation of physiological findings. There was no direct evidence that the PRC circuit is organized in this manner. The present study establishes that the differential impact of short- and long-range pathways depends on two complementary sources of inhibition that are expressed much more strongly in short- than in long-range pathways (Fig. 7A). This difference likely plays a major role in determining the impact of experience of perirhinal responses to complex stimuli. For instance, because cortical projections carrying different sensory modalities end at different rostrocaudal levels of the PRC (Fig. 7C), such an organization might underlie the perirhinal contributions to intermodal forms of associative memory (Parker and Gaffan, 1998; Goulet and Murray, 2001; Lindquist et al., 2004).

Acknowledgments

National Institutes of Health; Grant number: RO1 MH-073610 (to D.P.); Grant sponsor: National Center for Research Resources; Grant number: Yerkes Center base grant RR-00165.

Literature Cited

Apergis-Schoute J, Pinto A, Pare D. Muscarinic control of long-range GABAergic inhibition within the rhinal cortices. J Neurosci. 2007; 27:4061–4071. [PubMed: 17428984]

Barinka F, Salaj M, Rybář J, Krajčovičová E, Kubová H, Druga R. Calretinin, parvalbumin and calbindin immunoreactive interneurons in perirhinal cortex and temporal area Te3V of the rat brain: qualitative and quantitative analyses. Brain Res. 2012; 1436:68–80. [PubMed: 22221733]

Benson DL, Isackson PJ, Gall CM, Jones EG. Contrasting patterns in the localization of glutamic acid decarboxylase and Ca^{2+}/calmodulin protein kinase gene expression in the rat central nervous system. Neuroscience. 1992; 46:825–849. [PubMed: 1311814]

Biella G, Uva L, de Curtis M. Network activity evoked by neocortical stimulation in area 36 of the guinea pig perirhinal cortex. J Neurophysiol. 2001; 86:164–172. [PubMed: 11431498]

Biella G, Spaiardi P, Toselli M, de Curtis M, Gnatkovsky V. Functional interactions within the parahippocampal region revealed by voltage-sensitive dye imaging in the isolated guinea pig brain. J Neurophysiol. 2010; 103:725–732. [PubMed: 19939958]

Brown MW, Wilson FAW, Riches IP. Neuronal evidence that inferomedial temporal cortex is more important than hippocampus in certain processes underlying recognition memory. Brain Res. 1987; 409:158–167. [PubMed: 3107754]

Burwell RD, Amaral DG. Cortical afferents of the perirhinal, postrhinal, and entorhinal cortices of the rat. J Comp Neurol. 1998a; 398:179–205. [PubMed: 9700566]

Burwell RD, Amaral DG. Perirhinal and postrhinal cortices of the rat: interconnectivity and connections with the entorhinal cortex. J Comp Neurol. 1998b; 391:293–321. [PubMed: 9492202]

Ceranik K, Bender R, Geiger JR, Monyer H, Jonas P, Frotscher M, Lubke J. A novel type of GABAergic interneuron connecting the input and the output regions of the hippocampus. J Neurosci. 1997; 17:5380–5394. [PubMed: 9204922]

Cho K, Aggleton JP, Brown MW, Bashir ZI. An experimental test of the role of postsynaptic calcium levels in determining synaptic strength using perirhinal cortex of rat. J Physiol. 2001; 532:459–466. [PubMed: 11306664]

Colonnier, M. The electron-microscopic analysis of the neuronal organization of the cerebral cortex. In: Schmitt, FO.; Worden, FG.; Adelman, G.; Dennis, SG., editors. The organization of the cerebral cortex. Cambridge: MIT Press; 1981. p. 125-152.

Deacon TW, Eichenbaum H, Rosenberg P, Eckman KW. Afferent connections of the perirhinal cortex in the rat. J Comp Neurol. 1983; 220:168–190. [PubMed: 6643724]

DeFelipe J, Fariñas I. The pyramidal neuron of the cerebral cortex: morphological and chemical characteristics of the synaptic inputs. Prog Neurobiol. 1992; 39:563–607. [PubMed: 1410442]

Erondu NE, Kennedy MB. Regional distribution of type II Ca^{2+}/calmodulin-dependent protein kinase in rat brain. J Neurosci. 1985; 5:3270–3277. [PubMed: 4078628]

Fahy FL, Riches IP, Brown MW. Neuronal activity related to visual recognition memory: long-term memory and the encoding of recency and familiarity information in the primate anterior and medial inferior temporal cortex and rhinal cortex. Exp Brain Res. 1993; 96:457–472. [PubMed: 8299747]

Germroth P, Schwerdtfeger WK, Buhl EH. Gabaergic neurons in the entorhinal cortex project to the hippocampus. Brain Res. 1989; 494:187–192. [PubMed: 2765919]

Goulet S, Murray EA. Neural substrates of crossmodal association memory in monkeys: the amygdala versus the anterior rhinal cortex. Behav Neurosci. 2001; 115:271–284. [PubMed: 11345954]

Hughes CM, Peters A. Symmetric synapses formed by callosal afferents in rat visual cortex. Brain Res. 1992; 583:271–278. [PubMed: 1504833]

Jung SC, Kim J, Hoffman DA. Rapid, bidirectional remodeling of synaptic NMDA receptor subunit composition by A-type K channel activity in hippocampal CA1 pyramidal neurons. Neuron. 2008; 60:657–671. [PubMed: 19038222]

Lavenex P, Suzuki WA, Amaral DG. Perirhinal and parahippocampal cortices of the macaque monkey: Intrinsic projections and interconnections. J Comp Neurol. 2004; 472:371–394. [PubMed: 15065131]

Li L, Miller EK, Desimone R. The representation of stimulus familiarity in anterior inferior temporal cortex. J Neurophysiol. 1993; 69:1918–1929. [PubMed: 8350131]

Lindquist DH, Jarrard LE, Brown TH. Perirhinal cortex supports delay fear conditioning to rat ultrasonic social signals. J Neurosci. 2004; 24:3610–3617. [PubMed: 15071109]

Litman L, Awipi T, Davachi L. Category-specificity in the human medial temporal lobe cortex. Hippocampus. 2009; 19:308–319. [PubMed: 18988234]

Martina M, Royer S, Pare D. Propagation of neocortical inputs in the perirhinal cortex. J Neurosci. 2001; 21:2878–2888. [PubMed: 11306639]

Messinger A, Squire LR, Zola-Morgan S, Albright TD. Neuronal representations of stimulus associations develop in the temporal lobe during learning. Proc Natl Acad Sci USA. 2001; 98:12239–12244. [PubMed: 11572946]

Miller EK, Li L, Desimone R. Activity of neurons in anterior inferior temporal cortex during a short-term memory task. J Neurosci. 1993; 13:1460–1478. [PubMed: 8463829]

Naber PA, Witter MP, Lopes da Silva FH. Differential distribution of barrel or visual cortex evoked responses along the rostro-caudal axis of the peri- and post-rhinal cortices. Brain Res. 2000; 877:298–305. [PubMed: 10986344]

Naya Y, Yoshida M, Miyashita Y. Forward processing of long-term associative memory in monkey. J Neurosci. 2003; 23:2861–2871. [PubMed: 12684473]

Parker A, Gaffan D. Lesions of the primate rhinal cortex cause deficits in flavour-visual associative memory. Behav Brain Res. 1998; 93:99–105. [PubMed: 9659992]

Paxinos, G.; Watson, C. The rat brain in stereotaxic coordinates. New York: Academic Press; 2007.

Peters, A.; Palay, SL.; Webster, HF. The fine structure of the nervous system. New York: Oxford University Press; 1991.

Pinto A, Fuentes C, Pare D. Feedforward inhibition regulates perirhinal transmission of neocortical inputs to the entorhinal cortex: ultrastructural study in guinea pigs. J Comp Neurol. 2006; 495:722–734. [PubMed: 16506192]

Room P, Groenewegen HJ. Connections of the parahippocampal cortex. I. Cortical afferents. J Comp Neurol. 1986; 251:415–450. [PubMed: 2431008]

Sik A, Ylinen A, Penttonen M, Buzsáki G. Inhibitory CA1-CA3-hilar region feedback in the hippocampus. Science. 1994; 265:1722–1724. [PubMed: 8085161]

Smith Y, Pare D. Intra-amygdaloid projections of the lateral nucleus in the cat: PHA-L anterograde labeling combined with post-embedding GABA and glutamate immunocytochemistry. J Comp Neurol. 1994; 342:232–248. [PubMed: 7911130]

Sobotka S, Ringo JL. Investigation of long-term recognition and association memory in unit responses from inferotemporal cortex. Exp Brain Res. 1993; 96:28–38. [PubMed: 8243581]

Suzuki WA. The anatomy, physiology and functions of the perirhinal cortex. Curr Opin Neurobiol. 1996; 6:179–186. [PubMed: 8725959]

Suzuki WA, Amaral DG. Perirhinal and parahippocampal cortices of the macaque monkey: cortical afferents. J Comp Neurol. 1994; 350:497–533. [PubMed: 7890828]

Tighilet B, Hashikawa T, Jones EG. Cell- and lamina-specific expression and activity-dependent regulation of type II calcium/calmodulin-dependent protein kinase isoforms in monkey visual cortex. J Neurosci. 1998; 18:2129–2146. [PubMed: 9482799]

Unal G, Apergis-Schoute J, Pare D. Associative properties of the perirhinal cortex. Cereb Cortex. 2012; 22:1318–1332. [PubMed: 21841156]

Van Haeften T, Wouterlood FG, Jorritsma-Byham B, Witter MP. GABAergic presubicular projections to the medial entorhinal cortex of the rat. J Neurosci. 1997; 17:862–874. [PubMed: 8987807]

Van Haeften T, Baks-te-Bulte L, Goede PH, Wouterlood FG, Witter MP. Morphological and numerical analysis of synaptic interactions between neurons in deep and superficial layers of the entorhinal cortex of the rat. Hippocampus. 2003; 13:943–952. [PubMed: 14750656]

Witter MP, Room P, Groenewegen HJ, Lohman AHM. Connections of the parahippocampal cortex in the cat. V. Intrinsic connections; Comments on input/output connections with the hippocampus. J Comp Neurol. 1986; 252:78–94. [PubMed: 3793976]

Wouterlood FG, van Denderen JC, van Haeften T, Witter MP. Calretinin in the entorhinal cortex of the rat: distribution, morphology, ultrastructure of neurons, and co-localization with gamma-aminobutyric acid and parvalbumin. J Comp Neurol. 2000; 425:177–192. [PubMed: 10954838]

Wouterlood FG, Van Haeften T, Eijkhoudt M, Baks-Te-Bulte L, Goede PH, Witter MP. Input from the presubiculum to dendrites of layer-V neurons of the medial entorhinal cortex of the rat. Brain Res. 2004; 1013:1–12. [PubMed: 15196963]

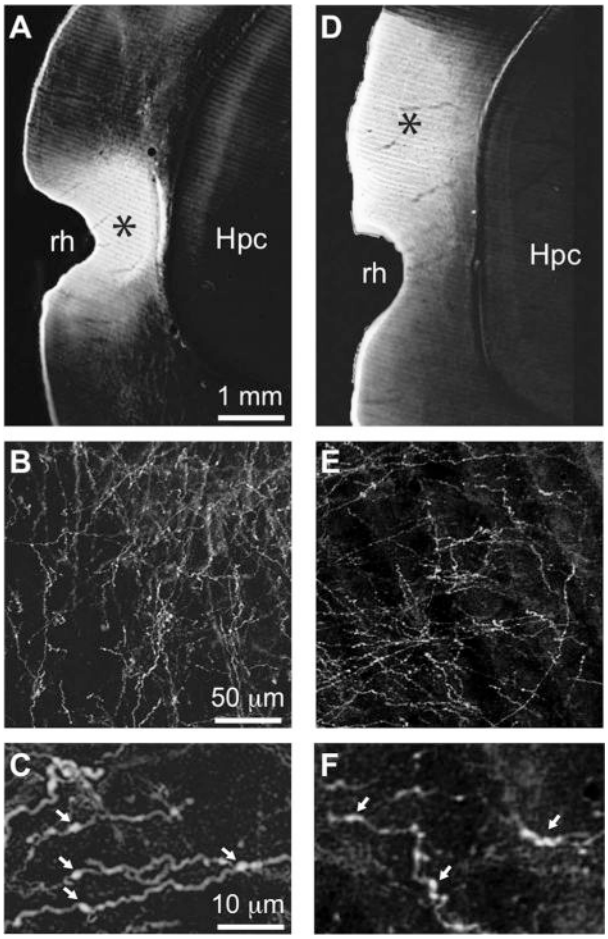

Figure 1.

Darkfield photomicrographs showing iontophoretic PHAL injections in the PRC (**A**) and VTAC (**D**) and of the resulting anterograde labeling (**B,C** and **E,F**, respectively). Asterisks in A and D indicate the core of PHAL injection sites. Low-power (B) and high-power (C) photomicrographs of anterograde labeling in area 35 of PRC following the PHAL injection shown in A. Low-power (E) and high-power (F) photomicrographs of anterograde labeling in area 36 of PRC following PHAL injection shown in D. Arrows in C and F point to axonal varicosities. Hpc, hippocampus; rh, rhinal sulcus. Scale bars = 1 mm in A (applies to A,D); 50 lm in B (applies to B,E); 10 μm in C (applies to C,F).

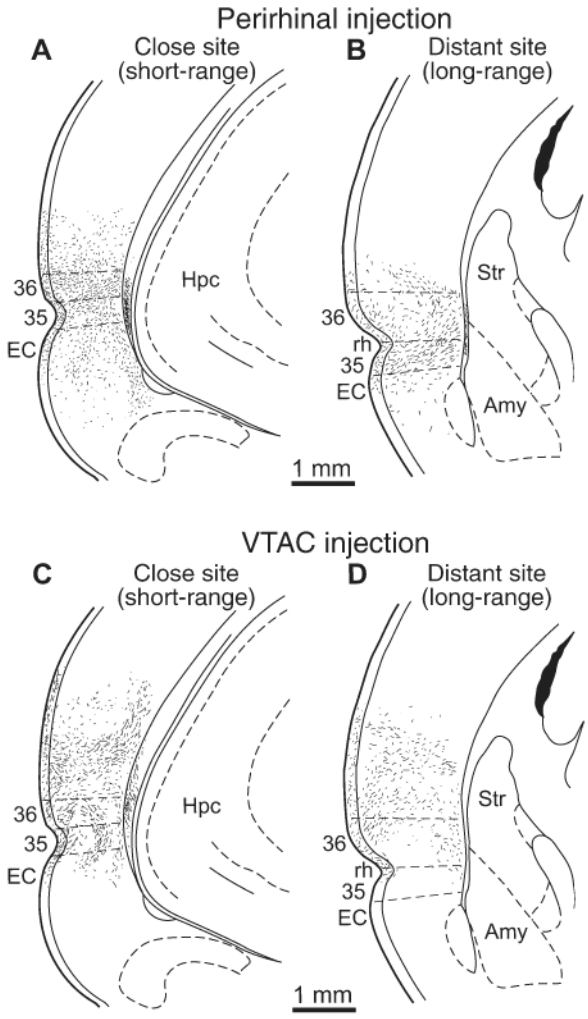

Figure 2.

Distribution of anterogradely labeled axons produced by PHAL injection in the caudal PRC (**A,B**) and VTAC (**C,D**). Schemes depict coronal sections close to (within 1 mm; A,C) and rostrocaudally distant from (B,D) the PHAL injection sites shown in Figure 1A,D, respectively. Dashed lines mark borders among VTAC, areas 36 and 35, as well as the entorhinal cortex. These were identified using a Nissl stain and based on prior descriptions of parvalbumin, calretinin, and calbindin immunoreactivity (Naber et al., 2000; Barinka et al., 2012). After both PHAL injections, the density of labeled axons was similar at perirhinal levels adjacent to the injection sites. In contrast, the density of PHAL-labeled axons was much lower at distant sites following the VTAC than the perirhinal injections. Note that anterograde labeling in sub-cortical structures, such as the amygdala and striatum, is not depicted. Amy, amygdala; EC, entorhinal cortex; Hpc, hippocampus; rh, rhinal sulcus; Str, striatum. Scale bars = 1 mm.

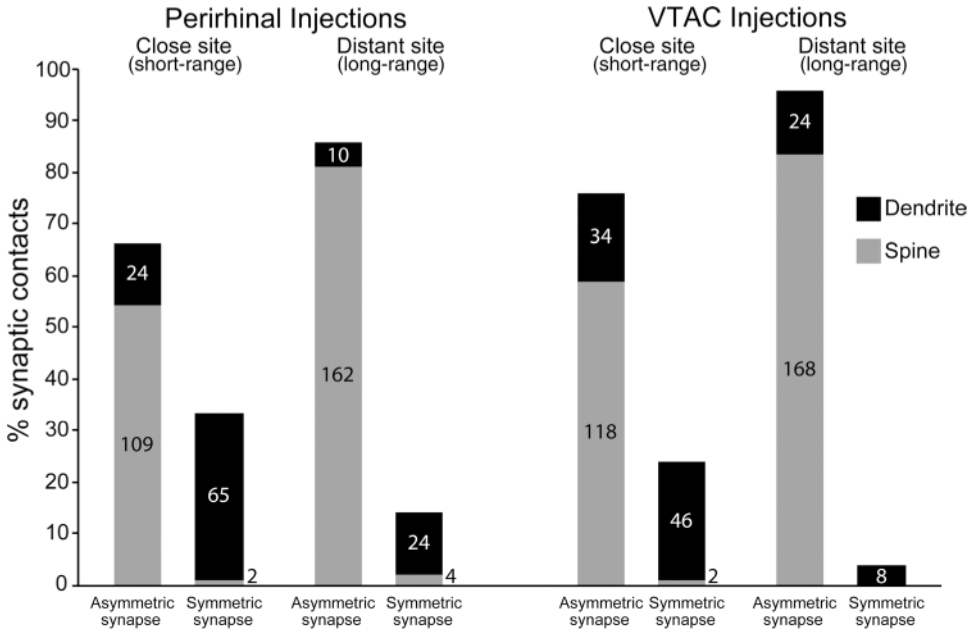

Figure 3.

Proportion of asymmetric vs. symmetric synapses and postsynaptic targets of PHAL-labeled axon terminals. Bar graph shows percentage of asymmetric and symmetric synapses observed following PRC (four leftmost bars) and VTAC (four rightmost bars) PHAL injections. In both injection groups, the first and last two bars, respectively, represent data obtained at perirhinal sites adjacent to and distant from the PHAL injection site. Numbers on the bars indicate the actual number of synapses analyzed in each condition. Each pair of bars, depicting asymmetric and symmetric synapses in a given site and injection group, includes a total of 200 synapses.

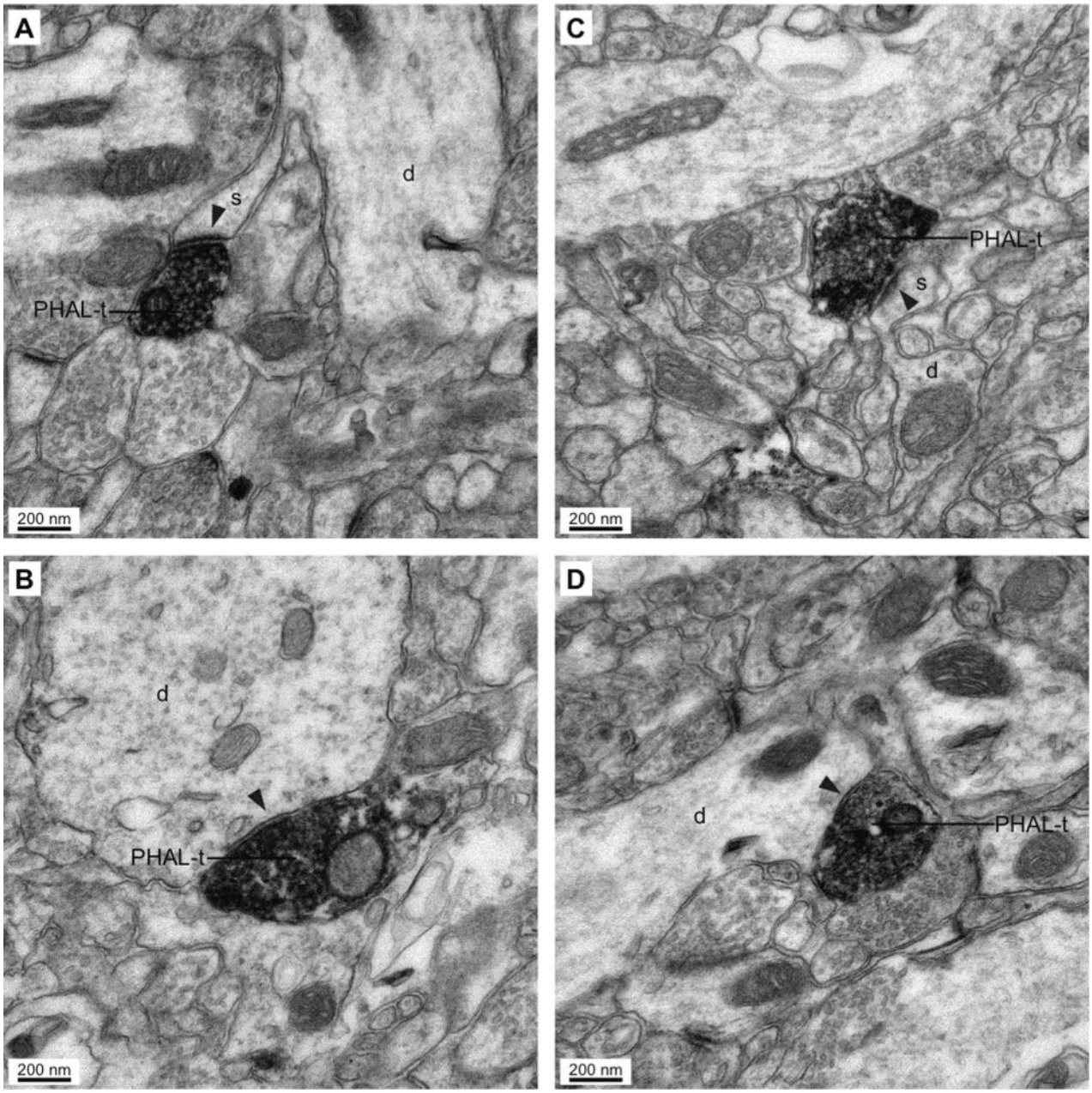

Figure 4.

Examples of synapses (arrowheads) formed by PHAL-labeled perirhinal (**A,B**) and VTAC (**C,D**) axon terminals (PHAL-t). Cases depicted in A and C show asymmetric synapses with dendritic spines. Cases depicted in B and D show symmetric synapses with dendritic profiles. d, Dendrite; s, spine. Scale bars = 200 nm.

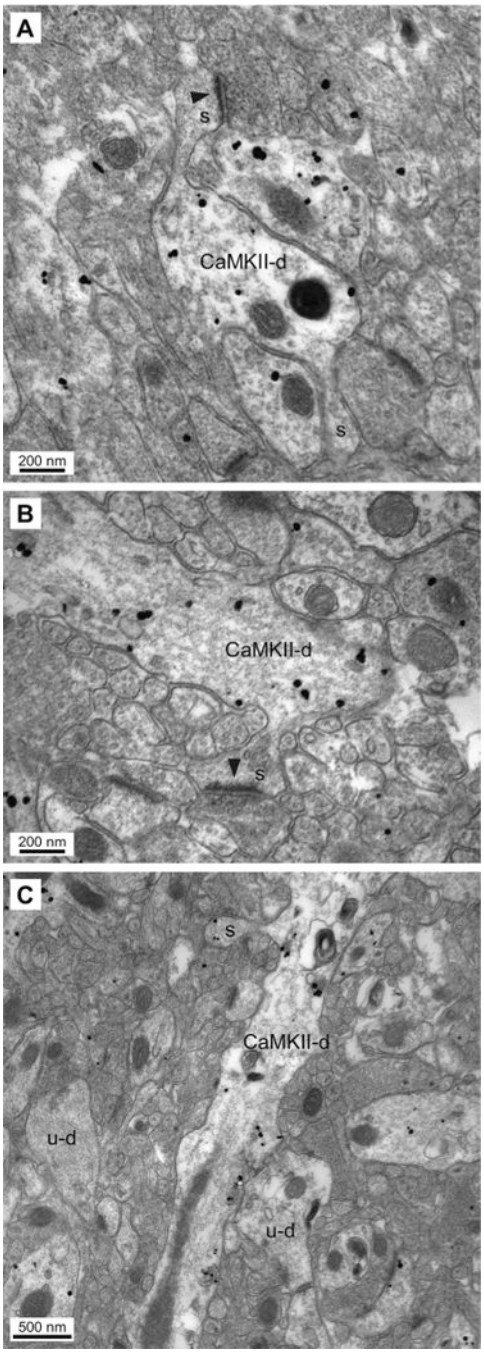

Figure 5.

Spiny dendrites are CaMKIIα immunoreactive. **A**–**C**: Electron micrographs showing dendritic profiles that are immunoreactive for CaMKIIα (CamKII-d) and from which emerge one or more spines (s). With the same material (C), we also observed aspiny dendritic profiles devoid of CaMKIIα immunoreactivity (u-d). Scale bars = 200 nm in A,B; 500 nm in C.

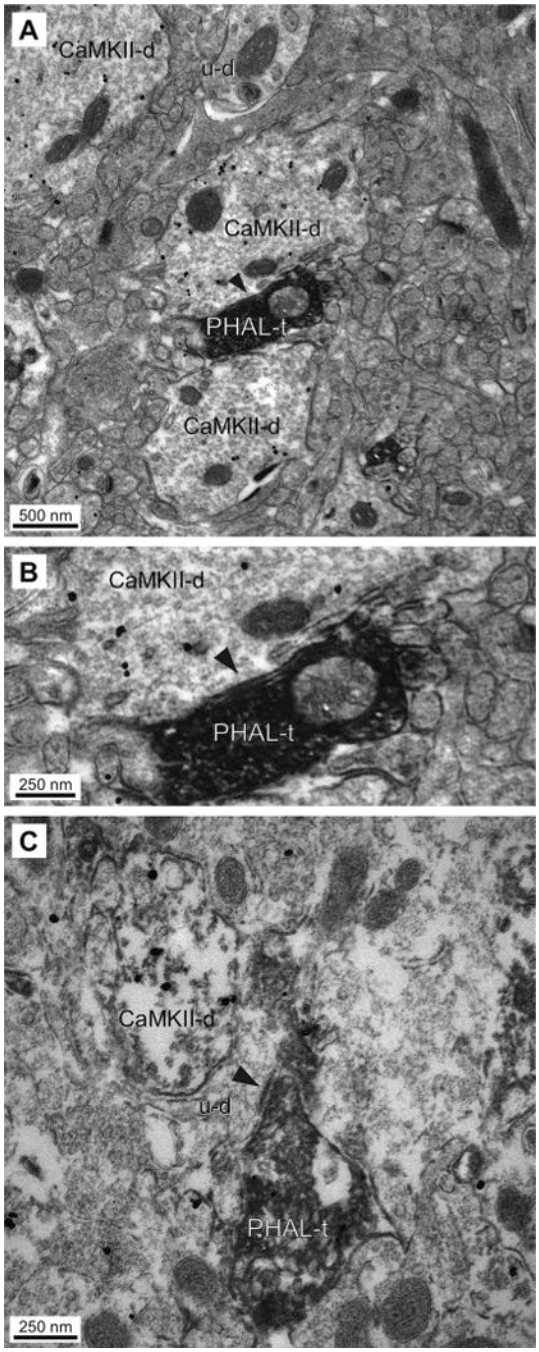

Figure 6.

Articulation of PHAL-positive axon terminals with CaMKIIa-immunopositive or -immunonegative elements. **A,B**: Electron micrographs showing, at different magnifications, PHAL-labeled axon terminal (PHAL-t) that forms a symmetric synapse (arrowhead) with a CaMKIIα-immunopositive dendrite (CaMKII-d). C: A PHAL-labeled axon terminal that forms an asymmetric synapse with a CaMKIIα-immunonegative dendritic profile (u-d). Scale bars = 500 nm in A; 250 nm in B,C.

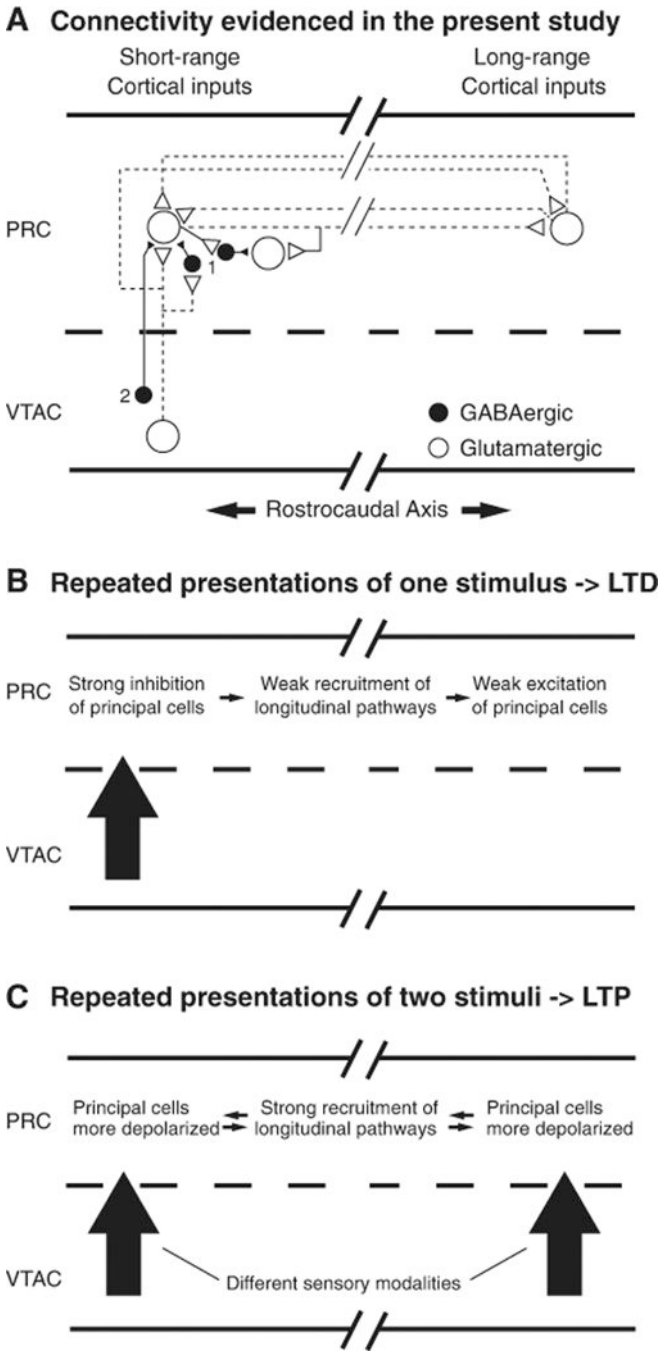

Figure 7.

Short- and long-range intracortical connections of perirhinal neurons and their possible significance for perirhinal contributions to memory. **A**: Scheme highlighting the different connections formed by short-range (left) and long-range (right) cortical inputs arising in the VTAC and PRC. Short-range pathways give rise to a larger contingent of inhibitory connections to PRC than long-range pathways. This inhibition takes two forms: 1) principal VTAC or perirhinal cells forming excitatory synapses with local-circuit inhibitory neurons of the PRC and 2) inhibitory neurons of the VTAC or PRC contacting principal perirhinal cells. **B,C**: Differential recruitment of longitudinal perirhinal pathways by spatially

circumscribed (B) vs. distributed (C) VTAC input patterns. In the first case (B), spatially circumscribed VTAC inputs cause a strong inhibition of principal perirhinal neurons, and, as a result, longitudinal pathways are weakly activated. It was shown that repeated presentations of such inputs cause LTD in vitro and a reduction of unit responses in vivo. In the second case (C), spatially distributed VTAC inputs recruit longitudinal perirhinal connections more strongly. Because longitudinal intrinsic axons recruit markedly less inhibition, they shift the balance of inhibition and excitation in favor of the latter. As a result, perirhinal cells are more depolarized, favoring the development of LTP in vitro and of increased responses to the paired stimuli in vivo.